Accepted for Publication in AJ
Preprint typeset using LaTeX style emulateapj v. 6/22/04

arXiv:1101.1082v2 [astro-ph.SR] 20 Jan 2011

# THE SLOAN DIGITAL SKY SURVEY DR7 SPECTROSCOPIC M DWARF CATALOG I: DATA

Andrew A. West[1,2,10], Dylan P. Morgan[2], John J. Bochanski[3,9], Jan Marie Andersen[2], Keaton J. Bell[4], Adam F. Kowalski[4], James R. A. Davenport[4], Suzanne L. Hawley[4], Sarah J. Schmidt[4], David Bernat[5], Eric J. Hilton[4], Philip Muirhead[5], Kevin R. Covey[2,5,6], Bárbara Rojas-Ayala[5], Everett Schlawin[5], Mary Gooding[7], Kyle Schluns[2], Saurav Dhital[8], J. Sebastian Pineda[3], David O. Jones[2]

*Accepted for Publication in AJ*

## ABSTRACT

We present a spectroscopic catalog of 70,841 visually inspected M dwarfs from the seventh data release of the Sloan Digital Sky Survey (SDSS). For each spectrum, we provide measurements of the spectral type, a number of molecular bandheads, and the H$\alpha$, H$\beta$, H$\gamma$, H$\delta$ and Ca II K emission lines. In addition, we calculate the metallicity-sensitive parameter $\zeta$ and identify a relationship between $\zeta$ and the $g-r$ and $r-z$ colors of M dwarfs. We assess the precision of our spectral types (which were assigned by individual examination), review the bulk attributes of the sample, and examine the magnetic activity properties of M dwarfs, in particular those traced by the higher order Balmer transitions. Our catalog is cross-matched to Two Micron All Sky Survey (2MASS) infrared data, and contains photometric distances for each star. Lastly, we identify eight new late-type M dwarfs that are possibly within 25 pc of the Sun. Future studies will use these data to thoroughly examine magnetic activity and kinematics in late-type M dwarfs and examine the chemical and dynamical history of the local Milky Way.

*Subject headings:* stars: low-mass — brown dwarfs — stars: activity — stars: late-type — stars: abundances — Galaxy: kinematics and dynamics

## 1. INTRODUCTION

Over the past decade, wide-field, deep astronomical surveys have provided an unprecedented statistical platform for studying the Universe (e.g. Sloan Digital Sky Survey, Two Micron All Sky Survey, 2dF, UKIRT Infrared Deep Sky Survey). For the lowest-mass and most populous stars in the Milky Way (M dwarfs), the Sloan Digital Sky Survey (SDSS) has yielded photometric samples that exceed 30 million stars (e.g. Bochanski et al. 2010) and spectroscopic samples of over 40,000 M and L dwarfs (West et al. 2008). Previous SDSS studies have elucidated the mean properties of low-mass stars (Hawley et al. 2002; West et al. 2004, 2005; Bochanski et al. 2007b; Schmidt et al. 2010b), their magnetic activity and flaring properties as a function of mass (West et al. 2004, 2008; Kowalski et al. 2009; Kruse et al. 2010; Hilton et al. 2010), as well as the structure and kinematics of the local Milky Way thin and thick disks (Bochanski et al. 2007a; Jurić et al. 2008; Fuchs et al. 2009; Bochanski et al. 2010) and the low-mass initial mass and luminosity functions (Covey et al. 2008b; Bochanski et al. 2010).

M dwarfs have main sequence lifetimes that are considerably longer than the age of the Universe and can be used to trace the evolution of both stellar properties and the Milky Way disks. West et al. (2006, 2008) showed that magnetic activity (as traced by H$\alpha$) in M dwarfs decreases with age and that M dwarfs appear to have finite activity lifetimes from ∼1-2 Gyr for early-type M dwarfs (M0-M3) to ∼7-8 Gyr for later type stars (M5-M7). These results are important for the habitability of extrasolar planets orbiting M dwarfs (e.g. Charbonneau et al. 2009), as active stars may disrupt planetary atmospheres (Segura et al. 2010). The H$\alpha$ emission does not have sufficient energy to significantly affect planetary systems but has been found to be correlate with X-ray emission (Reid et al. 1995b; Covey et al. 2008a), which can interact with extrasolar planet atmospheres.

While H$\alpha$ is the most commonly studied emission line in M dwarfs, the higher-energy hydrogen Balmer and Ca II transitions are also present in the optical spectra of active stars. The higher energy emission lines appear to trace different temperature regions in the chromosphere and can be used to characterize the upper atmospheres of active M dwarfs (Walkowicz & Hawley 2009, and references therein). However, lacking large samples of low-mass stars with spectroscopic coverage across the entire optical bandpass, it is still not clear how the various activity indicators trace each other in active M dwarfs (Rauscher & Marcy 2006; Walkowicz & Hawley 2009).

West et al. (2008, hereafter W08) also showed that the ratio of CaH/TiO molecular indices (a quantity that is likely related to metallicity; Gizis 1997) decreased with height in the Galactic disk (a proxy for age). This tantalizing result suggests that M dwarfs can be used to reconstruct the chemical evolution of the local Milky Way disk. However, the inability to assign accurate metallici-

---

[1] Corresponding author: aawest@bu.edu
[2] Department of Astronomy, Boston University, 725 Commonwealth Ave, Boston, MA 02215
[3] MIT Kavli Institute for Astrophysics and Space Research, 77 Massachusetts Ave, Cambridge, MA 02139-4307
[4] Department of Astronomy, University of Washington, Box 351580, Seattle, WA 98195
[5] Department of Astronomy, Cornell University, 610 Space Sciences Building, Ithaca, NY 14853
[6] Hubble Fellow
[7] Wells College, Department of Mathematical and Physical Sciences, 170 Main Street, Aurora, NY 13026
[8] Department of Physics and Astronomy, Vanderbilt University, 6301 Stevenson Center, Nashville, TN 37235
[9] Astronomy and Astrophysics Department, The Pennsylvania State University, 525 Davey Lab, University Park, PA 16802
[10] Visiting Investigator, Department of Terrestrial Magnetism, Carnegie Institute of Washington, 5241 Broad Branch Road, NW, Washington, DC 20015

ties to individual M dwarfs limits a detailed exploration of Galactic chemical evolution. Several recent studies have made progress in calibrating the M dwarf metallicity scale. Rojas-Ayala et al. (2010) used infrared spectroscopy of M dwarfs in wide binaries with higher-mass stars to calibrate infrared spectral features with metallicity. In the optical, Lépine et al. (2007) developed a metallicity-dependent quantity $\zeta$, which is a relation between the CaH and TiO molecular indices and defined as:

$$\zeta = \frac{1 - \mathrm{TiO5}}{1 - [\mathrm{TiO5}]_{Z_\odot}}, \tag{1}$$

where

$$\begin{aligned}[\mathrm{TiO5}]_{Z_\odot} = \quad & -0.164(\mathrm{CaH2} + \mathrm{CaH3})^3 \\ & +0.670(\mathrm{CaH2} + \mathrm{CaH3})^2 \\ & -0.118(\mathrm{CaH2} + \mathrm{CaH3}) - 0.050.\end{aligned} \tag{2}$$

Using wide binaries consisting of an M dwarf and a higher mass star, Woolf et al. (2009) showed that the $\zeta$ index is a good discriminant between high and low-metallicity ([Fe/H] =0 and [Fe/H] = -1 respectively) for early-type M dwarfs (∼M0-M3). While $\zeta$ is a useful tool for examining the relative metallicity among stars, finer determinations of an absolute metallicity from $\zeta$ will require additional calibration.

Before the SDSS (York et al. 2000), the largest spectroscopic samples of M dwarfs contained only a few thousand individual stars (Reid et al. 1995a) and were primarily focused on the red portion of the optical spectrum (∼6000-8000 Å). The spectroscopic catalogs of M dwarfs from the first few SDSS data releases quickly surpassed previous records for sample size (Hawley et al. 2002; West et al. 2004) and had spectral coverage that spanned the entire optical band (∼3900-9300 Å) at low resolution (R∼1800). W08 presented a spectroscopic catalog of more than 44,000 M dwarfs from the SDSS Data Release 5 (DR5), more than doubling the M dwarf spectroscopic tally. Due to the large number of spectra in the DR5 sample, spectral types were assigned using the Hammer[11] automatic spectral typing facility (Covey et al. 2007). While the Hammer spectral types are generally good to within ±1 sub–type, there have been recent indications that there may be systematic offsets for some of the M dwarf spectral types (see Section 2). Therefore, to ensure the highest quality sample, it is important to visually inspect each spectrum. There have been two subsequent SDSS data releases since the W08 sample that include over 50,000 additional M dwarf candidates and contain many sightlines at low Galactic latitudes (as part of the SEGUE survey; Yanny et al. 2009). The new lines of sight extend both the radial and vertical extent of the M dwarf sample, and provide a larger statistical platform from which to probe the structure, kinematics and evolution of the Milky Way using its smallest stellar constituents.

Here we present the latest spectroscopic catalog of M dwarfs from Data Release 7 (DR7; Abazajian et al. 2009) of the SDSS. While the main thrust of this paper is the presentation and characterization of a new spectroscopic sample, we have included a general magnetic activity analysis as well as a discussion about the future use of this sample to probe Galactic chemical evolution. We describe our sample selection techniques in Section 2, specifically discussing our manual inspection of *all* M dwarf candidates. Section 3 gives the mean properties of the sample, including a new activity analysis of the hydrogen Balmer and Ca II K emission features. Section 3 also contains a list of candidate M dwarfs within 25 pc and explores how the metallicity sensitive parameter $\zeta$ varies as a function of stellar parameters. We discuss our results and future use of our new sample in Section 4.

## 2. DATA AND SAMPLE SELECTION

The SDSS provides a large, uniform photometric and spectroscopic dataset from which to extract high-quality samples of low-mass dwarfs (Gunn et al. 1998; Fukugita et al. 1996; Hogg et al. 2001; Gunn et al. 2006; Ivezić et al. 2004; Pier et al. 2003; Smith et al. 2002; Tucker et al. 2006). We used the DR7 CasJobs[12] tool to select 116,161 M dwarf candidate objects with SDSS spectra that 1) fell within the typical color range for M and L dwarfs ($r-i > 0.42$ and $i-z > 0.24$; W08, Kowalski et al. 2009); 2) had SDSS spectral classifications of "STAR" or "STAR_LATE"; and 3) had radial velocities smaller than 1500 km s$^{-1}$. Kowalski et al. (2009) found that the color cuts used in previous studies did not extend blue enough ($r-i$ in particular) to include all of the M0 dwarfs. Our new (bluer) color selection corrects for this previous oversight.

The spectra for all 116,161 candidates were visually inspected and assigned spectral types using the Hammer spectral typing facility (Covey et al. 2007). Low signal-to-noise ratio (SNR) spectra (SNR <3 at ∼8300 Å) and extragalactic interlopers were removed during visual inspection, resulting in 109,639 objects. We also removed stellar spectra that were not identified as M dwarfs during visual inspection as well as those spectra that were duplicated in our sample (including 6771 spectra for 2661 M dwarfs that were taken on different days) and arrived at the 70,841 spectra of M dwarfs in our DR7 catalog. While many of the objects that we removed were K or L dwarfs, others were white dwarf–M dwarf (WD-dM) pairs and low-metallicity subdwarfs. All of the L dwarfs that were removed from our DR7 sample were cataloged and analyzed by Schmidt et al. (2010b). Many of the other objects that were not included in our DR7 sample will be presented in future studies. Not all of the WD-dM pairs were removed during the visual inspection. We used the color cuts from Smolčić et al. (2004, $u-g < 2$, $g-r > 0.3$, $r-i > 0.7$, $\sigma_{u,g,r,i} < 0.1$) to identify additional WD-dM pairs (that avoided manual detection). All of the 497 objects that matched these color criteria are flagged as "WDM" in our DR7 catalog. We also defined a clean photometric sample using the SDSS photometric processing flags (SATURATED, PEAKCENTER, NOTCHECKED, PSF_FLUX_INTERP, INTERP_CENTER, BAD_COUNTS_ERROR were all set to zero in the $r$, $i$, and $z$ bands)[13], which resulted in

---

[11] The Hammer software is available for public download at: http://astro.washington.edu/users/slh/hammer

[12] http://casjobs.sdss.org/

[13] http://www.sdss.org/dr7/products/catalogs/flags.html

65,277 M dwarfs. While our catalog contains all of the 70,84 visually inspected M dwarf spectra, the "GOODPHOT" and "WDM" flags can be used to obtain samples that include good photometry and remove possible WD-dM pairs respectively.

Radial velocities (RVs) were measured by cross-correlating each spectrum with the appropriate Bochanski et al. (2007b) M dwarf template. This method has been shown to produce uncertainties ranging from 7-10 km $s^{-1}$ (Bochanski et al. 2007b). All of the DR7 objects were cross-matched to the USNO-B/SDSS proper motion catalog (Munn et al. 2004, 2008), identifying 39,151 M dwarfs with good proper motions[14]. Distances to each star were calculated using the $M_r$ vs. $r-z$ color-magnitude relation given in Bochanski et al. (2010). Our calculated distances have uncertainties of ∼20%, arising mostly from the intrinsic spread of the main sequence. The proper motions and distances were combined with the RVs to produce 3-dimensional space motions for the DR7 M dwarfs. Although we include the standard $U$, $V$, $W$ space motions in our catalog, we caution that the $U$, $V$, $W$ velocities are in a Cartesian coordinate system that may not be appropriate for stars at appreciable distances from the Sun. We therefore also include the Galactic radial ($R$), tangential ($\Theta$) and vertical ($Z$) cylindrical components of the position and velocity for each star for which we have 3D space motions.

We also matched our catalog to the 2MASS point source catalog (Cutri et al. 2003), matching only to unique 2MASS counterparts within $5''$ of the SDSS position that do not fall within the boundaries of an extended source (GAL_CONTAM =0). To ensure that we used only high quality 2MASS photometric data, we applied additional cuts to each of the $J$, $H$, and $K_S$ bands. If the source was not detected (RD_FLG =0), nominally detected (RD_FLG =6), was detected but unresolved (RD_FLG =9), or had contaminated/confused photometry (CC_FLAG $\neq 0$) in a particular band, the 2MASS data were not included. This resulted in 57,956 2MASS counterparts with $J$, $H$ and $K_S$ magnitudes and their uncertainties that were included in the catalog.

We used the 2MASS photometry to investigate any possible M giant contamination. Bessell & Brett (1988) found that M giants and M dwarfs separate in $J-H$ vs. $H-K$ color space due to differences in $H_2O$ absorption in their atmospheres. By comparing the DR7 $J-H$ vs. $H-K$ color-color diagram with that of Bessell & Brett (1988), we find that no more than 0.5% of our sample could be giants. In addition, Covey et al. (2008b) conducted a complete magnitude-limited spectroscopic survey of a 1□° field in the SDSS footprint and concluded that the giant contamination rate was less than 2% for stars redder than a spectral type of K5.

### 2.1. *Spectral Typing*

Previous large spectroscopic samples of M dwarfs have relied on automated spectral typing due to the quantity of time required to manually inspect tens of thousands of candidate spectra. Systematic discrepancies were recently identified in the spectral types from the W08 SDSS sample that were determined automatically by the "Hammer" spectral typing algorithm (Covey et al. 2007). The bias was detected as a systematic offset for late-type stars, whose automatic classification was often 1 subtype earlier than determined via visual inspection (see Figure 1). We thus decided that visual inspection would produce the most reliable and precise spectroscopic sample. We visually inspected all 116,161 M dwarf candidates and manually assigned spectral types. The sample was divided among 17 individuals[15] who used the manual "eyecheck" mode of the Hammer (v. 1_2_5) to assign spectral types and remove non-M dwarf interlopers.

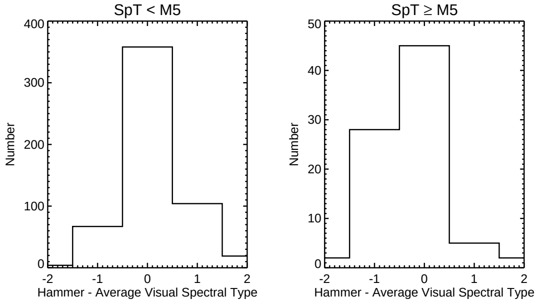

Fig. 1.— The distribution of differences between the Hammer automatic spectral types and the mean of the visually inspected spectral types for M dwarfs with visual types earlier than M5 (left) and M5 and later (right). While there is good agreement for the early-type M dwarfs, there is a systematic offset in the automatic types assigned by the Hammer; the Hammer assigns an earlier type ∼38% of the time.

Figure 1 shows the difference between the spectral types automatically determined by the Hammer and the mean visual inspection. For early-type M dwarfs (left panel), the Hammer and the spectral typers agree most of the time. However, for ∼38% of the late-type M dwarfs (right panel), the Hammer assigns spectral types 1 subtype earlier than the average human spectral typer. This confirms that while the Hammer generates automatic spectral types within the quoted ±1 subtype accuracy (Covey et al. 2007), there is a systematic offset of 1 subtype for the late-type stars, and justifies our effort to manually inspect more than 116,000 candidates.

Each spectral typer also examined a control sample of 1000 spectra, of which 638 were M dwarfs. We used this control sample to assess the quality and reliability of the visually inspected sample by quantifying the variations among the 17 individual typers, and by comparing the median visual type for each star to its automatic Hammer type. The results of the control sample show that there is excellent agreement between all of the spectral typers with a large fraction of the stars being assigned. Almost all of the visual classifications in the control sample agreed to within ±1 subtype of the median value; for most of the stars, the dispersion in visual classifications was $< 0.4$ subtypes. To ensure that there were no major systematics in the spectral types assigned by any individual, we examined the mean difference between each typer's visual classifications of the control sample spectra and the median classifications of the entire group. We divided the sample into the early types ($<$ M5) and late types ($\geq$ M5) to investigate any spectral type dependence in typing quality: all of the spectral typers clustered near the median values with no individual displaying a systematic offset larger than 0.2 subtypes.

---

[14] Good proper motions are defined as those with MATCH =1, DIST22 $>$ 7, SIGRA $<$ 1000, SIGDEC $<$ 1000 and (NFIT = 6 or (NFIT = 5 and (O $<$ 2 or J $<$ 2))) (Munn et al. 2004).

[15] The order of the co-authors was based on the number of spectra examined.

### 2.2. *Measured Quantities*

As part of our analysis we measured a number of spectral lines and molecular features in each M dwarf spectrum. All of the spectral measurements were made using the RV corrected spectra. The TiO1, TiO2, TiO3, TiO4, TiO5, TiO8, CaOH, CaH1, CaH2, and CaH3 molecular bandhead indices and their formal uncertainties were measured using the Hammer with the molecular bandheads as defined by Reid et al. (1995a) and Gizis (1997). We also measured the chromospheric hydrogen Balmer and Ca II lines that are associated with magnetic activity. We expanded the H$\alpha$ analysis of West et al. (2004, 2008) to include H$\beta$, H$\gamma$, H$\delta$ and Ca II K (H$\epsilon$ and Ca II H are blended in SDSS data and were not included in our sample). All of the line measurements were made by integrating over the specific line region (8 Å wide centered on the line) and subtracting off the mean flux calculated from two adjacent continuum regions (Continuum A and Continuum B in Table 1). Equivalent widths (EW) were computed for each line by dividing the integrated line flux by the mean continuum value (as in previous studies, we define the EW to be positive for emission lines; Hawley et al. 1996; West et al. 2004). The low-resolution of SDSS spectra does not affect our ability to measure accurate line values, with the exception of CaII K. Due to the intrinsic CaII K absorption present in M dwarf photospheres, weak activity appears as an emission peak in the absorption line. This weak emission cannot be resolved in SDSS spectra. However strong CaII K emission overwhelms the absorption and can be easily recovered from low-resolution spectra (Walkowicz & Hawley 2009). The lines and continuum regions (in vacuum wavelengths) can be found in Table 1. Formal uncertainties on the EWs for each line were also computed.

Similar to the West et al. (2004, 2008) samples, we defined magnetically active stars as those that had detectable emission lines in their spectra. Previously, this had been done solely for H$\alpha$. To be classified as active in a specific emission line, the following four criteria had to be satisfied: 1) the EW of the line was larger than some minimum value (see below); 2) the EW value must be 3 times the uncertainty; 3) the signal to noise ratio (SNR) in the continuum must be larger than 3; and 4) the height of the spectral line must be larger than 3 times the noise in the continuum. Stars were classified as inactive if they met criterion #3 and had no detectable emission. Criterion #3 preferentially selects brighter stars at any given color or spectral type. This selection bias should not have a large effect our results since we examine the properties of our sample in a Galactic context and both active and inactive stars with low SNR should be removed. However, if active stars are intrinsically more luminous than their inactive counterparts (at the same color; see Section 3.2 below), criterion #3 may serve to include slightly more active stars in our resulting analyses.

Because the strength of the stellar continuum changes dramatically from CaII K to H$\alpha$ in M dwarfs, the EW thresholds used in criterion #1 are different for each line. We experimentally derived the EW thresholds by automatically measuring activity in a subsample of 300 M dwarfs (that spanned a range of SNR and spectral types) using 10 different EW activity thresholds. Additionally, each spectrum was visually inspected and the activity state for all five emission lines was determined. By comparing the results of our manual inspection with the 10 different automatic routines, we determined the EW thresholds that most accurately reproduced our visual activity classifications. The EW activity threshold for each of the five emission lines can be found in Table 1. We found that the previous H$\alpha$ activity limit of 1 Å (West et al. 2004) was slightly too high and excluded a number of good detections. We have therefore reduced the H$\alpha$ EW activity criterion to 0.75 Å.

Recently, Kruse et al. (2010, hereafter K10) investigated the time variability of SDSS M dwarfs and defined their H$\alpha$ activity thresholds based on the median EW values that were detected at a $3\sigma$ confidence level as a function of spectral type. Although the K10 threshold EWs provide a robust way to select a clean sample, it unduly biases the sample toward the most active stars at later spectral types. For example, our DR7 catalog contains a large number of active M6 dwarfs (that have H$\alpha$ emission lines with peak values that are more than 5 times larger than the noise) that have EWs below the 3Å threshold used in the K10 study. In addition, the activity fractions presented in K10 (see their Figure 4) include these active stars (with EW $<$ 3Å) in the "inactive" component of the activity fraction denominator. This explains why the activity fractions reported by K10 are smaller than previous determinations (West et al. 2004, 2008) and indicates a serious selection bias in the K10 results.

For all of the active stars in the sample we computed the ratio of luminosity in the emission line as compared to the bolometric luminosity ($L_{\rm line}/L_{\rm bol}$). We followed the methods of Hall (1996), Walkowicz et al. (2004) and West & Hawley (2008) who derived $\chi$ factors for the Hydrogen Balmer and Ca II chromospheric lines as a function of M dwarf spectral type. The $\chi$ factor uses empirical results for the bolometric luminosities of M dwarfs as a function of color and/or spectral type (Leggett et al. 1996, 2001) and relates the EW of a line to the fraction of the bolometric luminosity emitted by the line. The $L_{\rm line}/L_{\rm bol}$ values were computed by multiplying the EW of each active star by the appropriate $\chi$ value. Formal uncertainties were computed for each $L_{\rm line}/L_{\rm bol}$ value and are included in the final database.

We also computed the metal sensitive parameter $\zeta$, defined by Lépine et al. (2007), which uses a combination of the TiO5, CaH2, and CaH3 molecular band indices to separate the sample into different metallicity classes (see Equations 1 & 2). This is similar to the Gizis (1997) classification system but was re-calibrated using wide common proper motion pairs that were assumed to be at the same metallicity. Stars with solar metallicity ([Fe/H]=0) have $\zeta$ values $\sim$1 and stars with [Fe/H]=-1 have $\zeta$ $\sim$0.4 (Woolf et al. 2009). Although there is considerable scatter in the [Fe/H] versus $\zeta$ relation at high-metallicities, this parameter is very useful for finding and classifying low-metallicity stars that are likely members of the Galactic halo.

Our catalog containing all of the measured quantities is

TABLE 1
EMISSION LINES

| Line | Central Wavelength (Å) | Continuum A (Å) | Continuum B (Å) | Activity Limit EW (Å) |
|---|---|---|---|---|
| H$\alpha$ | 6564.66 | 6555.0–6560.0 | 6570.0–6575.0 | 0.75 |
| H$\beta$ | 4862.69 | 4840.0–4850.0 | 4875.0-4885.0 | 1.00 |
| H$\gamma$ | 4341.69 | 4310.0–4330.0 | 4350.0–4370.0 | 1.00 |
| H$\delta$ | 4102.90 | 4075.0–4095.0 | 4110.0–4130.0 | 1.50 |
| CaII K | 3934.78 | 3952.8–3956.0 | 3974.0–3976.0 | 1.50 |

NOTE. — All of the wavelengths are given in vacuum units

publicly available on the Vizier[16] site or can be obtained by contacting the corresponding author. The individual spectra are available from the SDSS DR7 website[17]. As with previous SDSS spectroscopic catalogs of low-mass stars, we remind the community that these data do not represent a complete sample and that the complicated SDSS spectral targeting (see Section 3.1) introduces a variety of selection effects. However, our new sample covers a large range of values for many of the physical attributes of the M dwarfs, including parameters that are sensitive to activity, metallicity, and Galactic motion, making accurate activity, kinematic, and chemical analyses possible. In addition, because some of the derived quantities are computed by automatic routines, values for a small percentage (∼4%; West et al. 2004) of individual stars may be incorrect; this should not affect large statistical results. Users are nevertheless cautioned to understand the origin of specific data products before using them indiscriminately.

## 3. RESULTS

Figure 2 shows the distribution of spectral types for the DR7 low-mass star sample. We included the entire visually confirmed sample (solid), the stars for which we have good photometry (as indicated by our GOODPHOT flag; dotted), and the stars for which we have 3D kinematic information (as set by our GOODPM flag; dashed). A majority of the late-type M dwarfs are removed from the kinematic sample because they are too faint to be detected in the USNO-B catalog. Future studies will measure proper motions for the late-type M dwarfs in the DR7 catalog and create a more representative kinematic sample.

### 3.1. *Median Colors*

All of the magnitudes included in our DR7 catalog and used to compute the median colors were extinction corrected using the Schlegel et al. (1998) line-of-sight dust maps (and the dust model of Cardelli et al. 1989, and $R_V = 3.1$) . We provide extinction corrections for each band in the catalog so that observed magnitudes can be easily reproduced. Because of the close proximity of many of the M dwarfs in the sample, the entire Schlegel et al. (1998) extinction is likely an overestimate for many lines-of-sight. The uncertainty in the extinction correction introduces a small uncertainty in the derived distances. However, given the small amount of extinction toward objects in the SDSS footprint, the added uncertainties to the distances are typically less than 5%. We are currently determining the amount of extinction needed to reproduce an unreddened spectrum for each object in our DR7 sample, and will report on that analysis in a future paper (Jones et al. 2011).

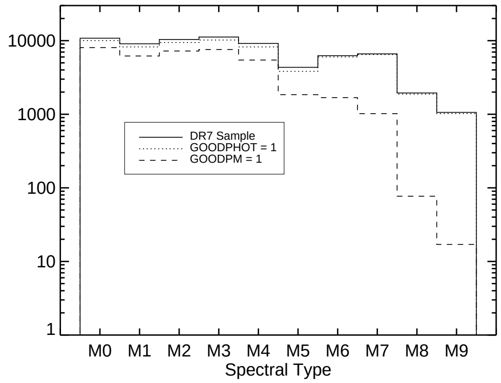

FIG. 2.— The distribution of spectral types in the spectroscopic SDSS DR7 M dwarf catalog (solid). The dotted line represents the stars for which good quality photometry exists (GOODPHOT = 1) and the dashed line indicates the stars for which good proper motions exist (GOODPM =1). Due to the shallow depths and blue sensitivity of the USNO-B catalog, there are only a small number of measured proper motions of the latest-type M dwarfs.

We computed median colors for each subtype of the DR7 sample, applying stringent cuts to include only those stars with the highest quality photometry. To be included in the median color calculation, SDSS stars had to have GOODPHOT = 1, $r$-band extinction <0.05 magnitudes, and $r$, $i$ and $z$-band magnitude uncertainties <0.05 magnitudes. Median colors incorporating 2MASS magnitudes were calculated from the subset of stars with $J$, $H$, and $K_S$ uncertainties <0.05. The median colors and standard deviations (in parentheses) are shown in Table 2. Due to the systematic offset in the Hammer automatic spectral types for late-type M dwarfs, our average colors are bluer than previously reported (W08, Kowalski et al. 2009). We include the $g - r$ colors but warn that they are likely metallicity dependent (West et al. 2004; Bochanski et al. 2007b, see also Section 3.3 below).

Figure 3 shows the $r$ versus $r - z$ Hess diagram for the M dwarfs in the SDSS DR7 sample. The gaps in color space reflect the non-uniform sampling due to the spectral targeting algorithm. To quantify the effect of

---

[16] http://vizier.u-strasbg.fr/cgi-bin/VizieR
[17] http://www.sdss.org/dr7

TABLE 2
MEDIAN COLORS

| Sp. Type | $N_{\rm SDSS}$[a] | $N_{\rm 2MASS}$[b] | $g-r$[c] | $r-i$ | $i-z$ | $z-J$ | $J-H$ | $H-K_S$ |
|---|---|---|---|---|---|---|---|---|
| M0 | 915 | 259 | 1.31 (0.16) | 0.56 (0.08) | 0.33 (0.06) | 1.20 (0.25) | 0.64 (0.07) | 0.16 (0.07) |
| M1 | 699 | 230 | 1.39 (0.16) | 0.73 (0.10) | 0.41 (0.08) | 1.32 (0.41) | 0.62 (0.08) | 0.19 (0.08) |
| M2 | 1078 | 689 | 1.40 (0.13) | 0.96 (0.10) | 0.53 (0.08) | 1.26 (0.18) | 0.60 (0.07) | 0.22 (0.08) |
| M3 | 1220 | 831 | 1.41 (0.13) | 1.13 (0.11) | 0.61 (0.08) | 1.30 (0.24) | 0.59 (0.06) | 0.23 (0.06) |
| M4 | 814 | 522 | 1.46 (0.15) | 1.33 (0.13) | 0.71 (0.09) | 1.37 (0.15) | 0.59 (0.06) | 0.25 (0.06) |
| M5 | 328 | 269 | 1.52 (0.13) | 1.62 (0.21) | 0.90 (0.13) | 1.47 (0.12) | 0.59 (0.06) | 0.28 (0.07) |
| M6 | 359 | 401 | 1.56 (0.15) | 1.92 (0.14) | 1.05 (0.07) | 1.61 (0.08) | 0.60 (0.06) | 0.31 (0.08) |
| M7 | 160 | 352 | 1.58 (0.16) | 2.09 (0.19) | 1.14 (0.10) | 1.71 (0.10) | 0.60 (0.08) | 0.34 (0.07) |
| M8 | 6 | 118 | 1.64 (0.12) | 2.56 (0.24) | 1.41 (0.13) | 1.93 (0.13) | 0.63 (0.07) | 0.39 (0.08) |
| M9 | 4 | 77 | 1.87 (0.74) | 2.70 (0.20) | 1.71 (0.18) | 2.15 (0.14) | 0.69 (0.09) | 0.42 (0.07) |

NOTE. — The median and rms scatter (in parentheses) of the extinction corrected SDSS-2MASS colors for each M dwarf spectral type. $u-g$ colors were not included due to the large uncertainties in the $u$-band photometry for most of the sample M dwarfs. The $g-r$ colors are included but are likely metallicity dependent (West et al. 2004; Bochanski et al. 2007b).

[a] The SDSS numbers reflect the stars that have good SDSS photometry (the GOODPHOT flag set to 1) and have $r$, $i$ and $z$ photometric uncertainties $< 0.05$ magnitudes.

[b] The 2MASS numbers indicate the number of stars that have $z$, $J$, $H$ and $K_S$-band uncertainties $< 0.05$ magnitudes.

[c] The $g-r$ colors were calculated using stars with good SDSS photometry (the GOODPHOT flag set to 1) and $g$ and $r$-band photometric uncertainties $< 0.05$ magnitudes.

SDSS spectroscopic targeting algorithms on the median colors, we conducted the following test. We began with the straw man assumption that the median $r-i$, $i-z$ and $r-z$ color-spectral type relations reported in Table 2 are representative of the underlying stellar population. We then used these quantities, along with the observed color spread in each spectral type bin, to construct a synthetic stellar population with a uniform distribution in both magnitude and spectral type. We then applied photometric cuts to the smooth underlying distribution, replicating the SDSS spectroscopic selection and producing a synthetic "observed" sample that is highly structured in color-magnitude space. The median colors and spreads were then calculated as a function of spectral type from this synthetic sample and compared to the measured colors in Table 2. In general, the colors of the synthetic stars agree to within 0.02 mags of the observed sample (an agreement that would not be expected if the underlying population were different from the observed SDSS stars ) and we conclude that the colors presented in Table 2 are not severely affected by the spectroscopic selection.

### 3.2. *Activity*

Figure 4 shows the H$\alpha$ activity fraction as a function of M dwarf spectral type for stars with data quality sufficient to measure H$\alpha$ emission (and GOODPHOT =1 and WDM =0). Our results are in good agreement with previous studies (West et al. 2004, W08), but with much lower uncertainties due to the ~59,000 M dwarfs used to generate Figure 4 (7952 are H$\alpha$ active and 51,034 are H$\alpha$ inactive). There are a few small differences between Figure 4 and the H$\alpha$ activity fractions reported by W08 that are likely due to the changes in some of the spectral types (see above) and the different Galactic sightlines included in the DR7 sample. Because of the lower SNR in the blue portion of M dwarfs, fewer stars were available to measure activity for the higher order Balmer and CaII K emission lines. Table 3 gives the number of active and inactive stars for each emission line indicator that had the necessary quality for our activity analysis.

As discussed in W08, the activity fraction is highly dependent on the location of the samples in the Galaxy. Because M dwarfs have finite activity lifetimes and are dynamically heated in the Galactic disk as they age, their activity state is correlated with position in the Galaxy. One of the reasons that the M dwarfs in our sample have much smaller activity fractions than those studied nearby (e.g. Hawley et al. 1996; Gizis et al. 2000), is that the SDSS volume is much larger than those used in previous catalogs and is concentrated on the north galactic cap, yielding a much older stellar population. This is particularly clear for the early-type M dwarfs, which have median distances greater than 500 pc, and therefore ages

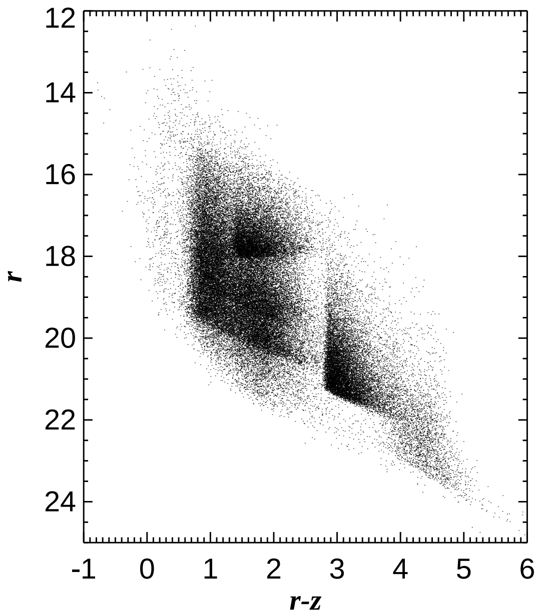

FIG. 3.— The $r$ versus $r-z$ Hess diagram for the M dwarfs in the SDSS DR7 sample. The gaps in color space reflect the non-uniform sampling due to the spectral targeting algorithm. The irregular sampling has a minimal effect on the median colors derived in the DR7 sample.

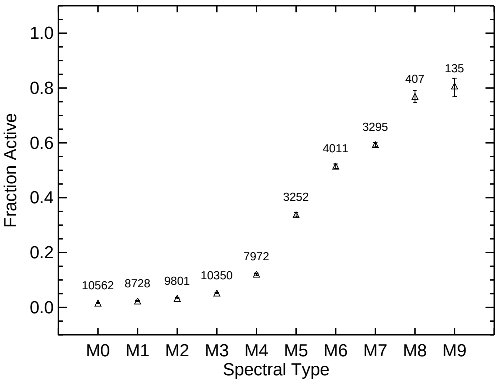

FIG. 4.— The H$\alpha$ magnetic activity fraction as a function of spectral type. Error bars were calculated from the binomial distribution and the number above each data point indicates the numbers of stars in that bin. See text for more details.

TABLE 3
ACTIVITY INDICATORS

| Line | $N_{\rm active}$ | $N_{\rm inactive}$ | Active Fraction |
|---|---|---|---|
| H$\alpha$ | 7952 | 51034 | 0.13 |
| H$\beta$ | 2236 | 35144 | 0.06 |
| H$\gamma$ | 1175 | 18816 | 0.06 |
| H$\delta$ | 528 | 14664 | 0.03 |
| CaII K | 620 | 9053 | 0.06 |

that are considerably older than their short activity lifetimes ($\sim$ 1-2 Gyr). We reiterate the warning from W08 that activity fractions in M dwarfs must be discussed in the proper Galactic context.

The various emission lines measured in our spectra are formed at slightly different locations in the chromosphere, suggesting that the strength of one emission line may not necessarily predict the strength of another. We therefore examined how the various activity induced emission lines trace each other as a function of spectral type and absolute distance from the Galactic plane (a proxy for age). Figure 5 shows the H$\alpha$ (diamonds) and H$\beta$ (asterisks) activity fractions for M2-M7 dwarfs as a function of Galactic height. Only the H$\alpha$ activity fractions for stars that could have detected H$\beta$ emission are included. This limits the sample to the brighter stars at each spectral type that meet the SNR criterion and does not include all of the M dwarfs that are sensitive to H$\alpha$ emission. Spectral types earlier than M2 and later than M7 were not included due to an insufficient sample size of active stars. As seen in previous studies, the magnetic activity fractions decrease as a function of Galactic height, confirming an age-activity relationship; stars closer to the Plane are statistically younger and more likely to be active. Figure 5 also demonstrates that H$\alpha$ and H$\beta$ trace each other extremely well for the entire DR7 sample, implying that the H$\beta$ activity lifetimes are essentially the same as those for H$\alpha$.

The other activity tracers also appear to correlate with H$\alpha$ emission. Figure 6 shows the activity fractions for all five emission lines in M4 dwarfs as a function of vertical distance from the Galactic plane. Each panel plots the activity fractions for stars where the data are good enough to measure (i.e. are sensitive to) H$\beta$ (top left), H$\gamma$ (top right), H$\delta$ (bottom left) and CaII K (bottom right) activity as well as the emission lines redder than that specific tracer. The activity fractions for all of the lines are in excellent agreement with each other and indicate that all five emission lines are produced for the same amount of time during the lifetime of an M dwarf. This new result is complementary to previous studies that found strong correlations among different emission line strengths in M dwarfs (Rauscher & Marcy 2006; Walkowicz & Hawley 2009). Although the relative emission line strengths for individual stars may fluctuate over time (see Cincunegui et al. 2007), the mean values of the emission lines are well correlated in the large DR7 sample. The unprecedented size and Galactic distribution of our spectroscopic sample confirms that not only the strength, but the duration of activity appears to be similar for all of the Balmer and CaII activity indicators.

Figure 6 also demonstrates a possible (and important) selection effect present in magnitude-limited or activity-selected samples. A close examination of Figure 6 (and Figure 5) reveals that the activity fractions are larger for the stars that are sensitive to the bluer emission lines. This trend was not expected since the stars used to compute the activity fraction were drawn from the same volumes in each of the four panels. The only difference was that the stars selected for the bluer emission line analyses were required to have higher SNR. With this in mind, we can explain the different activity fractions as follows.

The actual spread in absolute magnitude (or luminosity) at a given spectral type can be quite significant.[18] Some of this spread may be due to differences in the physical properties of the stars. Hawley et al. (1996) showed that magnetically active stars are brighter in $M_V$ than their inactive counterparts. Recently, Bochanski et al. (2011, hereafter Paper II) found that both active and higher metallicity M dwarfs (many stars are both) appear to be brighter in $M_r$ at a given color or spectral type. Because the bluer emission lines that we are examining in Figure 6 require higher SNR spectra to accurately measure activity, the M4 dwarfs at a given distance that meet the SNR criterion are preferentially more luminous than other stars in the same distance bin. If activity is correlated with luminosity, our SNR selection will bias our sample toward containing a higher fraction of active stars.

In addition to activity fractions, we also investigated the median luminosity in each emission line as a function of spectral type. Previous studies have investigated how the H$\alpha$ luminosity changes as a function of spectral type (Hawley et al. 1996; Gizis et al. 2000; Burgasser et al. 2002; West et al. 2004). These studies found that the fraction of luminosity emitted in H$\alpha$ is constant over the range M0-M5 and decreases by almost an order of magnitude for late-type M dwarfs. However, most of the previous studies concentrated on H$\alpha$ and did not include similar analyses for the other Balmer or CaII lines, and those that did were based on a small sample of stars (Hawley & Pettersen 1991; West & Hawley 2008).

---

[18] Recent studies have confirmed that the spread in absolute magnitude as a function of color is much smaller (Bochanski et al. 2010, 2011; Faherty et al. 2011). This is the primary reason that our distances are estimated from colors and not spectral types.

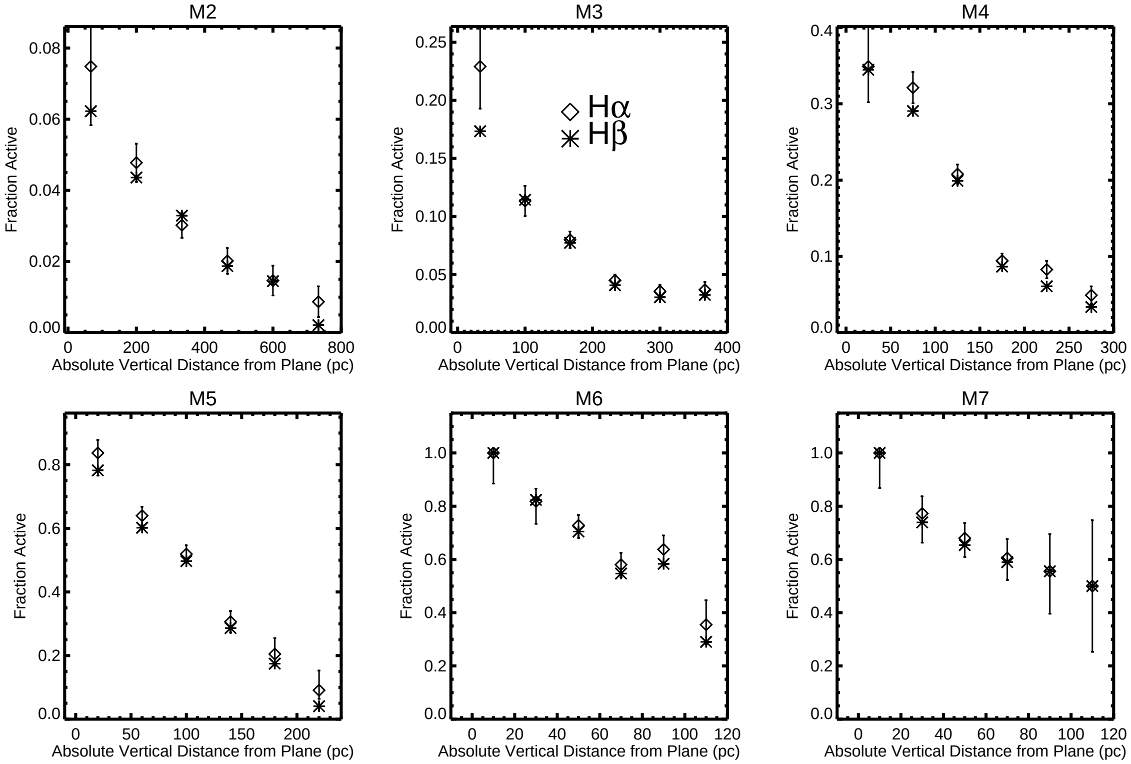

Fig. 5.— The Hα and Hβ activity fractions as a function of absolute vertical distance from the Galactic plane for M2–M7 dwarfs. For this comparison, only the stars with data good enough to measure Hβ were included. Error bars indicate the binomial errors in the Hα fractions – the Hβ uncertainties are similar. The Hβ activity fractions are in excellent agreement with the Hα data, indicating that Hβ activity has the same duration in M dwarfs.

Each panel of Figure 7 shows the median luminosity of a specific activity tracer (as compared to the bolometric luminosity of the stars) for active stars sensitive to that particular emission line. All of the activity tracers exhibit similar behavior, with the relative luminosity staying constant for the early-type M dwarfs and then falling to lower values at or around a spectral type of M5. The median values and the upper and lower quartiles that are plotted in Figure 7 are also given in Table 4. The bluer emission lines produce smaller fractional luminosities as expected, and are consistent with previous Balmer decrement studies (Hawley & Pettersen 1991; Bochanski et al. 2007b; West & Hawley 2008). W08 found evidence for a slight decrease in $L_{H\alpha}/L_{bol}$ as a function of Galactic height, but the effect is small and not included in our analysis.

### 3.3. *Metallicity Sensitive Features*

Metallicity continues to be one of the most elusive physical quantities to measure in M dwarfs. Recent work using infrared spectroscopy and improved photometry for M dwarfs in wide binaries may soon lead to accurate metallicity determinations for large samples of M dwarfs (Woolf et al. 2009; Johnson & Apps 2009; Rojas-Ayala et al. 2010). However, the Lépine et al. (2007) $\zeta$ parameter is currently the best indicator of metallicity in optical M dwarf spectra. Using the DR7 M dwarf sample, we examined how $\zeta$ changes as a function of Galactic height. Figure 8 shows median $\zeta$ values for M1 and M2 dwarfs as a function of absolute height above the Galactic plane. These specific spectral types were chosen because they span a large range of distance and contain a significant number of stars with $\zeta$ uncertainty $< 0.1$. Figure 8 shows a clear decrease in $\zeta$ for both spectral types with increasing Galactic height. The discrepancies in the nearby bins reflect the scatter in the high-metallicity end of the $\zeta$ vs. metallicity relation (Woolf et al. 2009). The results shown in Figure 8 suggest a significant change in the median metallicity of M dwarfs (and by extension the Galaxy) as a function of age, with the oldest stars (that are farther from the Plane) having the lowest metallicity. Similar trends have been seen in both the radial and vertical directions from previous spectroscopic samples of higher mass stars (Nordström et al. 2004; Ivezić et al. 2008). However, the higher density and longer main sequence lifetimes of M dwarfs may provide a better probe of the metal content (and evolution) of the local Galactic disk. The $\zeta$ values of ~0.6 in the most distant bins of Figure 8 have metallicities of [Fe/H]~-0.7 according to the wide binary analysis of Woolf et al. (2009).[19] We note that the photometric distances derived in our sample are likely affected by metallicity and that the farthest bins in Figure 8 (that have lower metallicities) are closer than shown due to fainter $M_r$ magnitudes (Paper II). Regardless, this strong trend in metallicity demonstrates the utility of large spectroscopic samples of M dwarfs (such as the one presented in this paper) for understanding the chemical evolution of the Milky Way. However,

[19] The Woolf et al. (2009) [Fe/H] – $\zeta$ calibration was limited to ~M0-M3 dwarfs and has considerable scatter at the high-metallicity end of the relation.

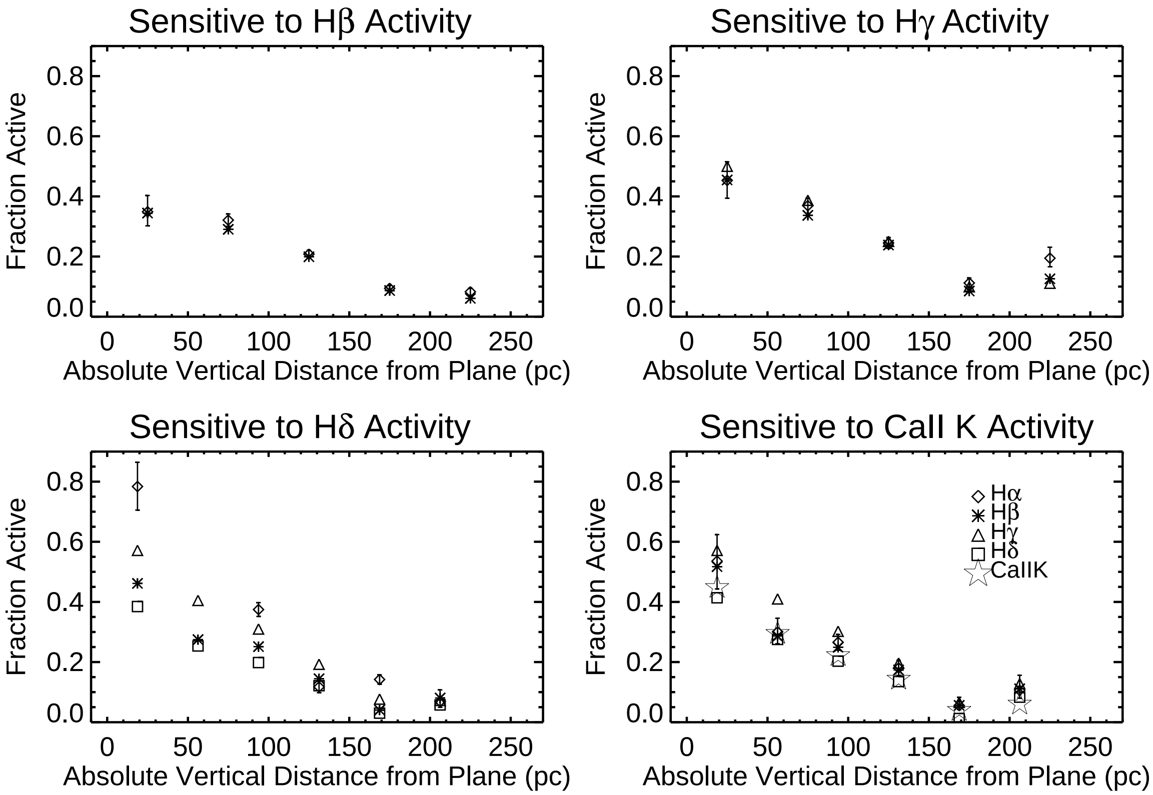

FIG. 6.— The H$\alpha$, H$\beta$, H$\gamma$, H$\delta$ and CaII K activity fractions for M4 dwarfs as a function of absolute vertical distance from the Galactic plane. Each panel includes only the stars where the data are good enough to be sensitive to that emission line (as well as all of the redder emission lines). Uncertainties are included for H$\alpha$ but are similar for all of the emission lines. The activity fractions have the same magnitude and decreasing trend with Galactic height for all lines. The activity fractions for stars sensitive to H$\delta$ and CaII K activity are slightly higher than for stars sensitive to H$\beta$ and H$\gamma$.

TABLE 4
LUMINOSITY IN ACTIVITY TRACER EMISSION LINES

| Spectral Type | $L_{\mathrm{H}\alpha}/\mathrm{L_{bol}}$ ($\times10^{-4}$) | $L_{\mathrm{H}\beta}/\mathrm{L_{bol}}$ ($\times10^{-4}$) | $L_{\mathrm{H}\gamma}/\mathrm{L_{bol}}$ ($\times10^{-4}$) | $L_{\mathrm{H}\delta}/\mathrm{L_{bol}}$ ($\times10^{-4}$) | $L_{\mathrm{CaII\ K}}/\mathrm{L_{bol}}$ ($\times10^{-4}$) |
|---|---|---|---|---|---|
| M0 | $1.27^{+0.39}_{-0.21}$ | $0.85^{+0.29}_{-0.17}$ | $0.50^{+0.13}_{-0.08}$ | $0.76^{+0.19}_{-0.46}$ | $0.33^{+0.07}_{-0.11}$ |
| M1 | $1.51^{+0.49}_{-0.35}$ | $0.81^{+0.28}_{-0.15}$ | $0.50^{+0.20}_{-0.13}$ | $0.39^{+0.09}_{-0.06}$ | $0.45^{+0.21}_{-0.14}$ |
| M2 | $1.42^{+0.45}_{-0.35}$ | $0.77^{+0.26}_{-0.24}$ | $0.44^{+0.15}_{-0.15}$ | $0.32^{+0.08}_{-0.09}$ | $0.34^{+0.18}_{-0.08}$ |
| M3 | $1.36^{+0.42}_{-0.42}$ | $0.67^{+0.22}_{-0.19}$ | $0.35^{+0.12}_{-0.11}$ | $0.26^{+0.10}_{-0.05}$ | $0.30^{+0.14}_{-0.15}$ |
| M4 | $1.44^{+0.63}_{-0.47}$ | $0.61^{+0.29}_{-0.22}$ | $0.35^{+0.14}_{-0.13}$ | $0.29^{+0.09}_{-0.10}$ | $0.28^{+0.11}_{-0.11}$ |
| M5 | $0.81^{+0.25}_{-0.22}$ | $0.33^{+0.11}_{-0.08}$ | $0.37^{+0.10}_{-0.11}$ | $0.26^{+0.07}_{-0.07}$ | $0.37^{+0.09}_{-0.15}$ |
| M6 | $0.57^{+0.20}_{-0.13}$ | $0.22^{+0.07}_{-0.06}$ | $0.13^{+0.02}_{-0.02}$ | $0.08^{+0.02}_{-0.02}$ | $0.17^{+0.04}_{-0.05}$ |
| M7 | $0.19^{+0.08}_{-0.05}$ | $0.06^{+0.03}_{-0.01}$ | $0.07^{+0.00}_{-0.03}$ | $0.06^{+0.02}_{-0.03}$ | $0.05^{+0.03}_{-0.03}$ |
| M8 | $0.27^{+0.12}_{-0.07}$ | $0.14^{+0.06}_{-0.05}$ | ... | ... | ... |
| M9 | $0.20^{+0.05}_{-0.06}$ | $0.12^{+0.14}_{-0.07}$ | ... | ... | ... |

NOTE. — Bolometrically scaled luminosities were derived using stars that show activity in each emission line. Reported uncertainties are the 25th and 75th quartile values.

additional calibration is required to convert quantities such as $\zeta$ into precise metallicities.

Previous SDSS studies have shown that the $g-r$ color of M dwarfs appears to correlate with metallicity (West et al. 2004; Lépine & Scholz 2008). Future large photometric surveys such as LSST (Ivezic et al. 2008) will rely heavily on the ability to classify objects based on their broadband colors alone. A large spectroscopic sample of M dwarfs, like the one presented here, can help correlate photometric properties of M dwarfs to spectroscopically derived physical parameters. Figure 9 shows the $g-r$ colors of M dwarfs as a function of $\zeta$ for M1-M4 dwarfs. Although there is a trend of decreasing $\zeta$ with redder $g-r$ color, the change in $g-r$ is different across spectral types. Therefore, $g-r$ color alone is not a good tracer of M dwarf metallicity across the range of M dwarf

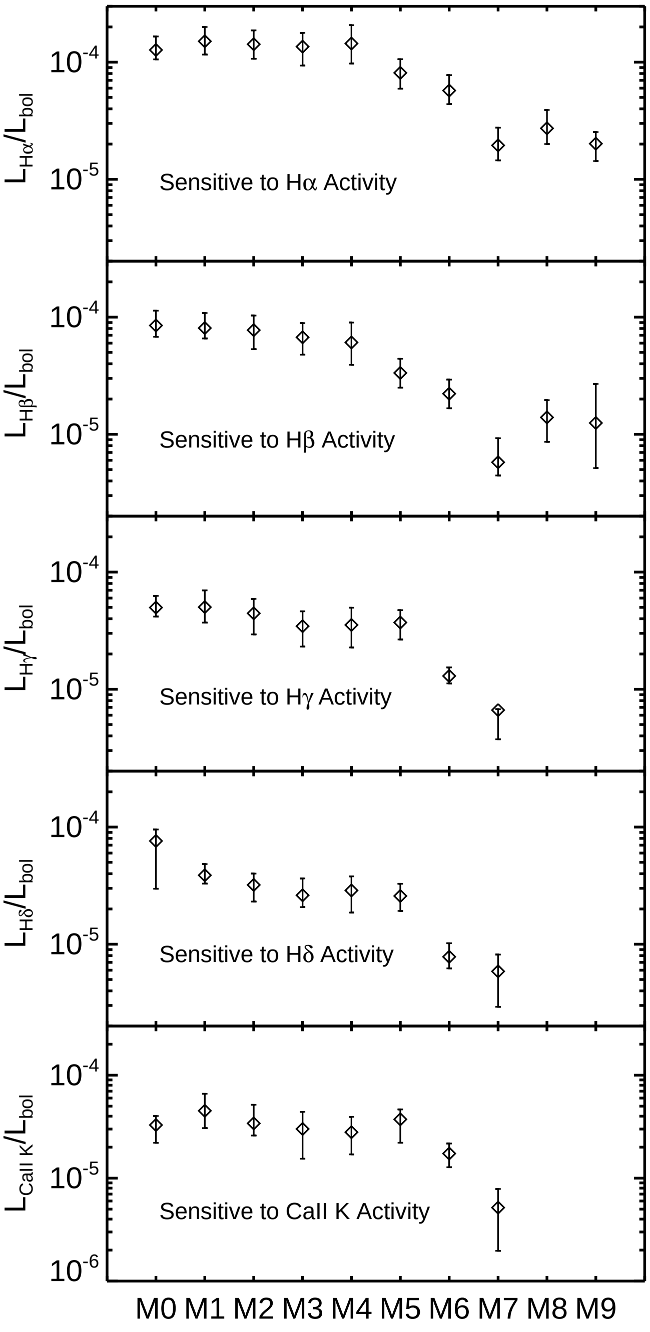

FIG. 7.— The ratio of line luminosity to bolometric luminosity as a function of spectral type for H$\alpha$, H$\beta$, H$\gamma$, H$\delta$ and Ca II K. The higher order Balmer and CaII K emission lines have progressively lower luminosity than the H$\alpha$ lines. All of the emission lines show a drop in the luminosity ratio for late-type M dwarfs.

spectral types. However, when we examined the $\zeta$ values as a function of both $g-r$ and $r-z$ (a proxy for spectral type; see Table 2), we found a strong trend of decreasing $\zeta$ diagonal to the $g-r$, $r-z$ axis and perpendicular to the stellar locus (Covey et al. 2007). Figure 10 highlights a region of color space that can be used to probe the metallicity content of M dwarfs and obtain low-metallicity members of the Galactic halo from solely broadband photometry. Using a Levenberg-Marquardt minimization technique, we derived a two-dimensional fit that relates $\zeta$ to the $g-r$ and $r-z$ colors:

$$\begin{aligned}\zeta = & 1.04 - 0.98(g-r)^2 - 0.07(r-z)^2 + 1.07(g-r) \\ & -0.53(r-z) + 0.63(g-r)(r-z). \qquad (3)\end{aligned}$$

Equation 3 is valid over the ranges shown in Figure 10 and has typical uncertainties of 10-20%.

### 3.4. *Nearby Stars*

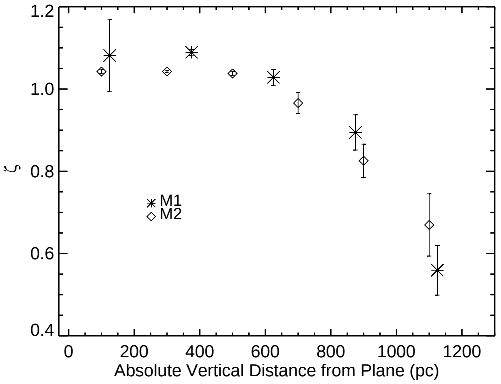

FIG. 8.— The metallicity dependent parameter $\zeta$ as a function of absolute height above the Galactic plane for M1 and M2 dwarfs. Metallicity decreases at large Galactic heights uniformly for both spectral types, indicating a significant evolution of M dwarf metallicity in the Galactic disk. The error bars reflect the uncertainty in the median values in each bin. This trend, along with the ubiquity and longevity of M dwarfs, paves the way for future studies of the chemical evolution of the nearby Milky Way.

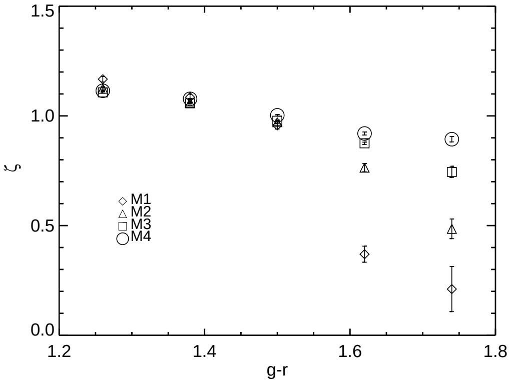

FIG. 9.— The metallicity sensitive parameter $\zeta$ as a function of $g-r$ color for M1-M4 stars. While $\zeta$ decreases at redder $g-r$ colors, the decrease is not uniform across spectral type.

Prompted by the discovery of new low-mass stars in the solar vicinity from other SDSS studies (e.g. Schmidt et al. 2010a), we inspected our catalog for M dwarfs that are possibly within 25 pc of the Sun. We found 21 nearby M dwarf candidates (8 of which were previously unidentified) based on the distances derived using the $M_r$, $r-z$ photometric parallax relation of Bochanski et al. (2010). Three of the stars were in the W08 SDSS DR5 sample but were not identified there as potential solar neighbors. Table 5 gives the positions, spectral types and distance estimates for all 21 of the nearby candidates. The closest candidate is SDSS1410+1846, which has an estimated distance of 14.8 pc. Since roughly one out of every 1000 M dwarfs in SDSS has a spectrum, there is a strong possibility that many more nearby stars await discovery and will be cataloged in future studies.

## 4. CONCLUSIONS

We have presented the SDSS DR7 M dwarf spectroscopic catalog, which consists of more than 70,000 visually confirmed M dwarfs and represents the largest spectroscopic sample of M dwarfs ever assembled. Our value-added catalog includes proper motions, RVs, photometric matches to 2MASS, spectral classification, distances, calculated space velocities, activity-induced emission line measurements and molecular bandhead strengths. The DR7 catalog is available for download at the Vizier site or by contacting the corresponding author. Our analysis of the visual spectral classification as compared to the automatic Hammer results reveals a slight $\sim 0.4$ subtype systematic offset in the automatic Hammer spectral types for late-type M dwarfs but confirms that the automatic types are good to within the stated precision of 1 spectral subtype. We present updated median colors for all M dwarf spectral types.

We have also analyzed some of the bulk properties of the DR7 sample. The main results of our analysis are as follows:

1. The magnetic activity fractions of low-mass stars as traced by H$\beta$, H$\gamma$, H$\delta$, and CaII K, decrease as a function of Galactic height and agree with those previously traced using H$\alpha$. This confirms that the presence and duration of magnetic activity as traced by the higher order Balmer emission lines and CaII K is similar to that of H$\alpha$, albeit at lower line luminosities and only measured in stars with sufficient SNR.

2. The metallicity sensitive parameter $\zeta$ decreases as a function of Galactic height, confirming a decline in the metal content of distant M dwarfs (and the Galactic disk) as a function of age.

3. As previously shown, the $g-r$ color of M dwarfs correlates with metallicity (here parameterized by $\zeta$). However, the $g-r$ versus $\zeta$ relation *is* spectral type dependent. Using both the $g-r$ and $r-z$ colors, we demonstrate that low-metallicity subdwarfs can be identified using photometry alone. This relation will be useful for source identification in upcoming large photometric surveys such as Pan-STARRS and LSST.

4. The DR7 M dwarf sample contains several previously unidentified M dwarfs that are likely within 25 pc of the Sun, including one that is possibly closer than 15 pc. The sparse spectroscopic coverage of low-mass stars in SDSS suggests that there are numerous M dwarf solar neighbors that will be identified in future studies. The advent of large, multi-epoch, deep surveys will be particularly useful for completing the nearby M dwarf census.

Many additional studies will make use of our M dwarf catalog. Those already underway include a statistical parallax analysis of absolute magnitude variations in the M dwarf population (Paper II), a detailed examination of M dwarf kinematics and the motions of the Galactic thin and thick disks (Pineda et al. 2011, Paper III), and an investigation of the content and distribution of dust in the local Galaxy (Jones et al. 2011). In addition to the current and unforeseen science that will be accomplished with our sample, we anticipate that our M dwarf catalog will be used to select and classify M dwarfs in several upcoming large surveys. Over 1 billion M dwarfs will be observed and cataloged in the new wave of large

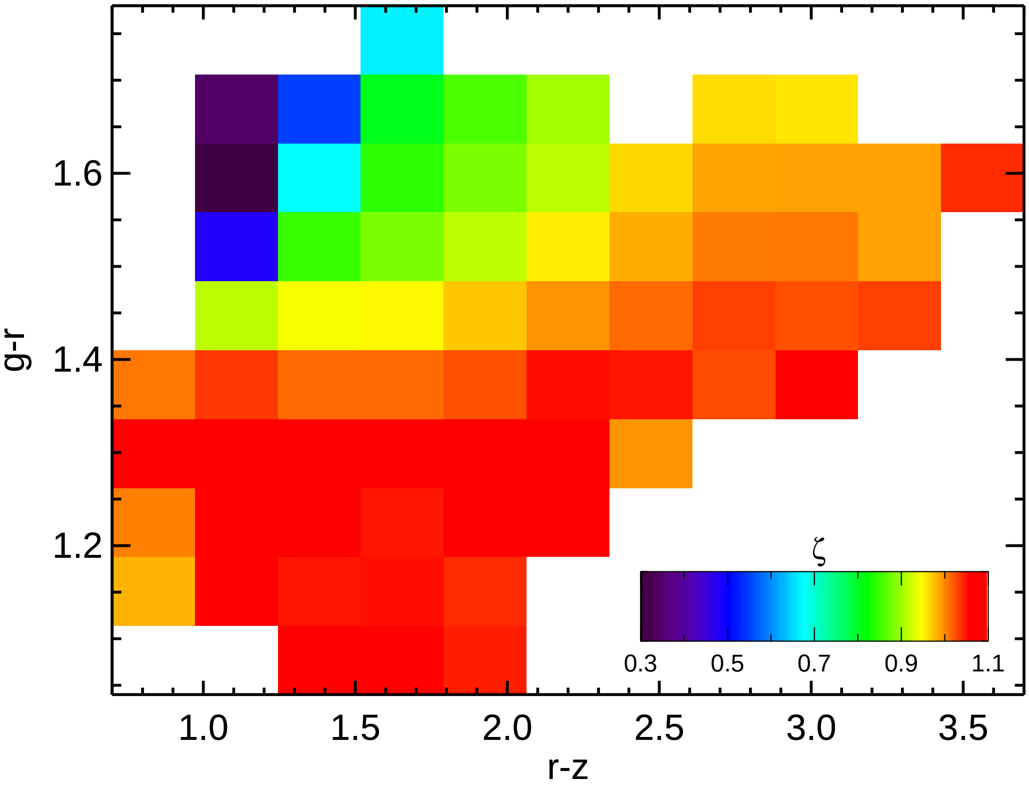

FIG. 10.— The $g - r$ versus $r - z$ colors of M dwarfs in the DR7 spectroscopic sample. The bins have been color coded according to their $\zeta$ values. Metallicity decreases along roughly diagonal lines in the $g - r$, $r - z$ color space and perpendicular to the stellar locus (Covey et al. 2007). This relation should be useful for classifying M dwarfs and identifying low-metallicity subdwarfs in upcoming large photometric surveys.

photometric surveys coming online in the next decade. We hope that our large M dwarf sample presented in this paper will provide a useful tool for correlating the spectroscopic attributes of low-mass stars with their photometric properties both in single exposures and in the time domain.

The authors would like to thank Sebastian Lépine, Jackie Faherty, Adam Burgasser, Evgenya Shkolnik and Edo Berger for useful discussions leading to the completion of this catalog. The authors also thank the anonymous referee for his/her insightful comments, which greatly improved the quality of the original manuscript. S.L.H. and J.J.B. acknowledge the support of NSF AST grant 06-07644. K.R.C. acknowledges support for this work from the Hubble Fellowship Program, provided by NASA through Hubble Fellowship grant HST-HF-51253.01-A awarded by the STScI, which is operated by the AURA, Inc., for NASA, under contract NAS 5-26555.

Funding for the Sloan Digital Sky Survey (SDSS) and SDSS-II has been provided by the Alfred P. Sloan Foundation, the Participating Institutions, the National Science Foundation, the U.S. Department of Energy, the National Aeronautics and Space Administration, the Japanese Monbukagakusho, and the Max Planck Society, and the Higher Education Funding Council for England. The SDSS Web site is http://www.sdss.org/.

The SDSS is managed by the Astrophysical Research Consortium (ARC) for the Participating Institutions. The Participating Institutions are the American Museum of Natural History, Astrophysical Institute Potsdam, University of Basel, University of Cambridge, Case Western Reserve University, The University of Chicago, Drexel University, Fermilab, the Institute for Advanced Study, the Japan Participation Group, The Johns Hopkins University, the Joint Institute for Nuclear Astrophysics, the Kavli Institute for Particle Astrophysics and Cosmology, the Korean Scientist Group, the Chinese Academy of Sciences (LAMOST), Los Alamos National Laboratory, the Max-Planck-Institute for Astronomy (MPIA), the Max-Planck-Institute for Astrophysics (MPA), New Mexico State University, Ohio State University, University of Pittsburgh, University of Portsmouth, Princeton University, the United States Naval Observatory, and the University of Washington.

This publication makes use of data products from the Two Micron All Sky Survey, which is a joint project of the University of Massachusetts and the Infrared Processing and Analysis Center/California Institute of Technology, funded by the National Aeronautics and Space Administration and the National Science Foundation.

## REFERENCES

Abazajian, K. N., et al. 2009, ApJS, 182, 543
Berger, E., et al. 2008, ApJ, 673, 1080

TABLE 5
M Dwarf Candidates Within 25 pc

| Name | Distance[a] (pc) | Spectral Type | R.A. (J2000) h | m | s | Dec. (J2000) ° | ′ | ″ | ref. |
|---|---|---|---|---|---|---|---|---|---|
| SDSS0013−0025 | 23.6 | M7 | 00 | 13 | 09.33 | −00 | 25 | 52.0 | 1, 4 |
| SDSS0124−0027 | 22.8 | M7 | 01 | 24 | 31.25 | −00 | 27 | 56.3 | 7 |
| SDSS0312+0021 | 24.9 | M7 | 03 | 12 | 25.13 | 00 | 21 | 58.4 | new |
| SDSS0351−0052 | 13.5 | M7 | 03 | 51 | 00.03 | −00 | 52 | 45.9 | 6 |
| SDSS0830+0947 | 20.8 | M9 | 08 | 30 | 32.37 | 09 | 47 | 12.7 | 10 |
| SDSS0902+0033 | 20.2 | M8 | 09 | 02 | 06.91 | 00 | 33 | 19.4 | 1 |
| SDSS0911+2248 | 21.9 | M7 | 09 | 11 | 30.54 | 22 | 48 | 10.8 | new |
| SDSS1003−0105 | 21.2 | M8 | 10 | 03 | 19.15 | −01 | 05 | 08.0 | 1, 8 |
| SDSS1016+2751 | 18.3 | M8 | 10 | 16 | 34.61 | 27 | 51 | 46.5 | 9, 10 |
| SDSS1119+0820 | 24.7 | M8 | 11 | 19 | 46.53 | 08 | 20 | 35.1 | 1, 2 |
| SDSS1134+2046 | 16.5 | M6 | 11 | 34 | 15.72 | 20 | 46 | 54.2 | 5 |
| SDSS1252+0252 | 23.5 | M8 | 12 | 52 | 22.63 | 02 | 52 | 05.7 | 1, 2 |
| SDSS1253+4034 | 21.1 | M7 | 12 | 53 | 12.49 | 40 | 34 | 00.6 | 1, 9, 10 |
| SDSS1326+5640 | 18.0 | M7 | 13 | 26 | 16.31 | 56 | 40 | 44.7 | 1 |
| SDSS1336+4751 | 23.9 | M8 | 13 | 36 | 50.50 | 47 | 51 | 32.2 | 1 |
| SDSS1410+1846 | 14.8 | M6 | 14 | 10 | 10.41 | 18 | 46 | 12.0 | new |
| SDSS1422+2116 | 21.7 | M8 | 14 | 22 | 24.27 | 21 | 16 | 07.6 | new |
| SDSS1440+1339 | 24.1 | M7 | 14 | 40 | 22.87 | 13 | 39 | 20.8 | 10 |
| SDSS1500−0039 | 21.5 | M7 | 15 | 00 | 26.35 | −00 | 39 | 27.9 | new |
| SDSS1501+2250 | 19.9 | M9 | 15 | 01 | 08.17 | 22 | 50 | 01.8 | 11, 12 |
| SDSS1627+3538 | 24.7 | M7 | 16 | 27 | 18.20 | 35 | 38 | 35.7 | 1, 2, 3 |

Note. — (1) W08; (2) Lépine & Shara (2005); (3) West & Basri (2009); (4) Branham (2003); (5) Luyten (1979); (6) Gliese & Jahreiß (1991); (7) Salim & Gould (2003); (8) Deacon et al. (2005); (9) Cruz et al. (2003) ; (10) Schmidt et al. (2007); (11) Berger et al. (2008); (12) Dahn et al. (2002)

[a] Photometric distances estimated using the $M_r$, $r - z$ relation from Bochanski et al. (2010).

Bessell, M. S., & Brett, J. M. 1988, PASP, 100, 1134

Bochanski, J. J., Hawley, S. L., Covey, K. R., West, A. A., Reid, I. N., Golimowski, D. A., & Ivezić, Ž. 2010, AJ, 139, 2679

Bochanski, J. J., Hawley, S. L., & West, A. A. 2011, AJ, submitted

Bochanski, J. J., Munn, J. A., Hawley, S. L., West, A. A., Covey, K. R., & Schneider, D. P. 2007a, AJ, 134, 2418

Bochanski, J. J., West, A. A., Hawley, S. L., & Covey, K. R. 2007b, AJ, 133, 531

Branham, Jr., R. L. 2003, Ap&SS, 288, 417

Burgasser, A. J., Liebert, J., Kirkpatrick, J. D., & Gizis, J. E. 2002, AJ, 123, 2744

Cardelli, J. A., Clayton, G. C., & Mathis, J. S. 1989, ApJ, 345, 245

Charbonneau, D., et al. 2009, Nature, 462, 891

Cincunegui, C., Díaz, R. F., & Mauas, P. J. D. 2007, A&A, 469, 309

Covey, K. R., et al. 2007, AJ, 134, 2398

—. 2008a, ApJS, 178, 339

—. 2008b, AJ, 136, 1778

Cruz, K. L., Reid, I. N., Liebert, J., Kirkpatrick, J. D., & Lowrance, P. J. 2003, AJ, 126, 2421

Cutri, R. M., et al. 2003, 2MASS All Sky Catalog of point sources.

Dahn, C. C., et al. 2002, AJ, 124, 1170

Deacon, N. R., Hambly, N. C., & Cooke, J. A. 2005, A&A, 435, 363

Faherty, J., et al. 2011, AJ, submitted

Fuchs, B., et al. 2009, AJ, 137, 4149

Fukugita, M., Ichikawa, T., Gunn, J. E., Doi, M., Shimasaku, K., & Schneider, D. P. 1996, AJ, 111, 1748

Gizis, J. E. 1997, AJ, 113, 806

Gizis, J. E., Monet, D. G., Reid, I. N., Kirkpatrick, J. D., Liebert, J., & Williams, R. J. 2000, AJ, 120, 1085

Gliese, W., & Jahreiß, H. 1991, Preliminary Version of the Third Catalogue of Nearby Stars, Tech. rep.

Gunn, J. E., et al. 1998, AJ, 116, 3040

—. 2006, AJ, 131, 2332

Hall, J. C. 1996, PASP, 108, 313

Hawley, S. L., Gizis, J. E., & Reid, I. N. 1996, AJ, 112, 2799

Hawley, S. L., & Pettersen, B. R. 1991, ApJ, 378, 725

Hawley, S. L., et al. 2002, AJ, 123, 3409

Hilton, E. J., West, A. A., Hawley, S. L., & Kowalski, A. F. 2010, ArXiv e-prints

Hogg, D. W., Finkbeiner, D. P., Schlegel, D. J., & Gunn, J. E. 2001, AJ, 122, 2129

Ivezić, Ž., et al. 2004, Astronomische Nachrichten, 325, 583

Ivezic, Z., et al. 2008, Serbian Astronomical Journal, 176, 1

Ivezić, Ž., et al. 2008, ApJ, 684, 287

Johnson, J. A., & Apps, K. 2009, ApJ, 699, 933

Jones, D., West, A. A., & Foster, J. 2011, AJ, submitted

Jurić, M., et al. 2008, ApJ, 673, 864

Kowalski, A. F., Hawley, S. L., Hilton, E. J., Becker, A. C., West, A. A., Bochanski, J. J., & Sesar, B. 2009, AJ, 138, 633

Kruse, E. A., Berger, E., Knapp, G. R., Laskar, T., Gunn, J. E., Loomis, C. P., Lupton, R. H., & Schlegel, D. J. 2010, ApJ, 722, 1352

Leggett, S. K., Allard, F., Berriman, G., Dahn, C. C., & Hauschildt, P. H. 1996, ApJS, 104, 117

Leggett, S. K., Allard, F., Geballe, T. R., Hauschildt, P. H., & Schweitzer, A. 2001, ApJ, 548, 908

Lépine, S., Rich, R. M., & Shara, M. M. 2007, ApJ, 669, 1235

Lépine, S., & Scholz, R. 2008, ApJ, 681, L33

Lépine, S., & Shara, M. M. 2005, AJ, 129, 1483

Luyten, W. J. 1979, LHS catalogue. A catalogue of stars with proper motions exceeding 0”5 annually, ed. Luyten, W. J.

Munn, J. A., et al. 2004, AJ, 127, 3034

—. 2008, AJ, 136, 895

Nordström, B., et al. 2004, A&A, 418, 989

Pier, J. R., Munn, J. A., Hindsley, R. B., Hennessy, G. S., Kent, S. M., Lupton, R. H., & Ivezić, Ž. 2003, AJ, 125, 1559

Pineda, J. S., West, A. A., Bochanski, J. J., & Burgaser, A. J. 2011, AJ, submitted

Rauscher, E., & Marcy, G. W. 2006, PASP, 118, 617

Reid, I. N., Hawley, S. L., & Gizis, J. E. 1995a, AJ, 110, 1838

Reid, N., Hawley, S. L., & Mateo, M. 1995b, MNRAS, 272, 828

Rojas-Ayala, B., Covey, K. R., Muirhead, P. S., & Lloyd, J. P. 2010, ApJ, 720, L113

Salim, S., & Gould, A. 2003, ApJ, 582, 1011

Schlegel, D. J., Finkbeiner, D. P., & Davis, M. 1998, ApJ, 500, 525

Schmidt, S. J., Cruz, K. L., Bongiorno, B. J., Liebert, J., & Reid, I. N. 2007, AJ, 133, 2258
Schmidt, S. J., West, A. A., Burgasser, A. J., Bochanski, J. J., & Hawley, S. L. 2010a, AJ, 139, 1045
Schmidt, S. J., West, A. A., Hawley, S. L., & Pineda, J. S. 2010b, AJ, 139, 1808
Segura, A., Walkowicz, L., Meadows, V., Kasting, J., & Hawley, S. 2010, ArXiv e-prints
Smith, J. A., et al. 2002, AJ, 123, 2121
Smolčić, V., et al. 2004, ApJ, 615, L141
Tucker, D. L., et al. 2006, Astronomische Nachrichten, 327, 821
Walkowicz, L. M., & Hawley, S. L. 2009, AJ, 137, 3297
Walkowicz, L. M., Hawley, S. L., & West, A. A. 2004, PASP, 116, 1105
West, A. A., & Basri, G. 2009, ApJ, 693, 1283
West, A. A., Bochanski, J. J., Hawley, S. L., Cruz, K. L., Covey, K. R., Silvestri, N. M., Reid, I. N., & Liebert, J. 2006, AJ, 132, 2507
West, A. A., & Hawley, S. L. 2008, PASP, 120, 1161
West, A. A., Hawley, S. L., Bochanski, J. J., Covey, K. R., Reid, I. N., Dhital, S., Hilton, E. J., & Masuda, M. 2008, AJ, 135, 785
West, A. A., Walkowicz, L. M., & Hawley, S. L. 2005, PASP, 117, 706
West, A. A., et al. 2004, AJ, 128, 426
Woolf, V. M., Lépine, S., & Wallerstein, G. 2009, PASP, 121, 117
Yanny, B., et al. 2009, AJ, 137, 4377
York, D. G., et al. 2000, AJ, 120, 1579